

Influence of Ba-to-Si deposition rate ratios on the electrical and optical properties of B-doped BaSi₂ epitaxial films

Shu Sugiyama, Yudai Yamashita, Kaoru Toko, and Takashi Suemasu

Institute of Applied Physics, University of Tsukuba, Tsukuba, Ibaraki 305-8573, Japan

Abstract

BaSi₂ is considered a candidate for a light absorbing layer of a solar cell. The carrier type, carrier density, and photoresponsivity of undoped BaSi₂ films depend on Ba-to-Si deposition rate ratios ($R_{\text{Ba}}/R_{\text{Si}}$) during molecular beam epitaxy (MBE). In this study, we examined these properties of B-doped BaSi₂ epitaxial films grown by MBE. We fabricated 0.5- μm -thick lightly B-doped BaSi₂ epitaxial films on Si (111) substrates at a substrate temperature of 600 °C. $R_{\text{Ba}}/R_{\text{Si}}$ was varied in the range 1.0–5.6 and the B concentration was set at about 10^{16} cm^{-3} . The p-type BaSi₂ films were formed only in the range of $R_{\text{Ba}}/R_{\text{Si}} = 2.1\text{--}2.9$, whereas BaSi₂ formed with other values of $R_{\text{Ba}}/R_{\text{Si}}$ showed n-type conductivity. The photoresponsivity significantly depended on $R_{\text{Ba}}/R_{\text{Si}}$, and reached values higher than those obtained for undoped BaSi₂ films. We ascribed the enhancement of photoresponsivity to B atoms making Si vacancies inactive in B-doped BaSi₂ films.

I. INTRODUCTION

Currently, crystalline Si solar cells occupy more than 90% of the solar cell market. However, its conversion efficiency η has reached 26.7% at the research stage.¹⁾ This value is close to the theoretical limit.²⁾ Therefore, various materials have been extensively studied for solar cell applications. Solar cells using III-V compound semiconductors such as GaAs achieve higher η than Si solar cells.³⁾ However, those solar cells are expensive and therefore larger-scale deployment is not easy. Under these circumstances, we have focused on orthorhombic BaSi₂ as a solar cell material which can be fabricated on a Si substrate.⁴⁻⁶⁾ BaSi₂ is a rare earth-free and nontoxic semiconductor. Besides, it consists of abundant elements, Ba and Si. BaSi₂ possesses a suitable bandgap (1.3 eV) for a single-junction solar cell, and a high optical absorption coefficient $\alpha = 3 \times 10^4 \text{ cm}^{-1}$ at 1.5 eV, which is more than 40 times as large as that of crystalline Si.⁷⁻¹⁰⁾ Moreover, its minority carrier diffusion length is about 10 μm ,¹¹⁾ which is sufficiently large as a thin film solar cell material. Due to these attractive features, BaSi₂ is expected to be a new candidate for high- η thin film solar cells. So far, various properties of BaSi₂ films have been investigated. Regarding control of carrier type and carrier concentration, we succeeded to control hole and electron concentrations in the range $10^{16} - 10^{19} \text{ cm}^{-3}$ by using B and Sb as dopants, respectively.¹²⁻¹⁴⁾ In addition, we achieved a large minority carrier lifetime ($\tau \sim 10 \mu\text{s}$) thanks to a-Si passivation layers.¹⁵⁻¹⁷⁾ By using these techniques, we have achieved η approaching 10% in p-BaSi₂/n-Si heterojunction solar cells.¹⁸⁻²⁰⁾ This value is the highest ever achieved for solar cells using semiconducting silicides. As a next step, we target to achieve BaSi₂ homojunction solar cells.²¹⁾ Recently, we have demonstrated the operation of homojunction solar cells, wherein the optical absorbing layer was lightly B-doped BaSi₂.^{21,22)} However, the η was as low as 0.28%.²²⁾ We attribute such a small η

to defects in the BaSi₂ light absorbing layer. First-principle calculations based on VASP code show that Si vacancies (V_{Si}) are most likely to occur in BaSi₂ regardless of BaSi₂ formed under Si-rich or Si-poor (Ba-rich) conditions,²³⁾ and V_{Si} form localized states within the bandgap, and thereby acts as recombination centers. Thus, we need to fabricate high-quality BaSi₂ epitaxial films with a low defect density. In our previous study,²⁴⁾ it was proven that Ba-to-Si deposition rate ratios ($R_{\text{Ba}}/R_{\text{Si}}$) during molecular beam epitaxy (MBE) has an enormous impact on carrier type, carrier concentration, and photoresponsivity. Especially, in the case of undoped BaSi₂ ones, the carrier concentration reached a minimum and therefore the photoconductivity reached a maximum at $R_{\text{Ba}}/R_{\text{Si}} = 2.2$ when grown at 580 °C.²⁴⁾ Therefore it is considered reasonable that the electrical and optical properties of lightly B-doped BaSi₂ epitaxial films depend also on $R_{\text{Ba}}/R_{\text{Si}}$. In this study, we fabricated lightly B-doped BaSi₂ epitaxial films using various values of $R_{\text{Ba}}/R_{\text{Si}} = 1.0\text{--}5.6$ on Si (111) substrates and evaluated their electrical and optical properties.

II. EXPERIMENTAL METHOD

We fabricated lightly B-doped BaSi₂ epitaxial films on Si (111) substrates with MBE system equipped with an electron-beam evaporation source for 10N-Si and standard Knudsen cells for 3N-Ba and B. We used floating-zone (FZ) n-Si(111) substrates (resistivity $\rho > 10000 \text{ } \Omega\text{cm}$) for Hall-effect measurement and microwave-detected photoconductivity decay (μ -PCD) measurement. On the other hand, we used Czochralski (CZ) n-Si(111) substrate ($\rho < 0.01 \text{ } \Omega\cdot\text{cm}$) for photoresponsivity measurement. Before fabricating the BaSi₂ epitaxial films, we cleaned the Si substrate surfaces by RCA (Radio Corporation of America) procedure so that we can cover the surface with a protective

oxide layer. Then, we removed the oxide layer by heating the substrate at a temperature (T_s) of 900°C in the ultra-high vacuum chamber. Next, we formed 5-nm-thick BaSi₂ template layers by depositing Ba on a Si substrate at $T_s = 500$ °C.²⁵⁾ We call this procedure reactive deposition epitaxy. Under this procedure, R_{Ba} was set at 1 nm/min. After that, we grew 0.5- μ m-thick B-doped BaSi₂ films on the templates by MBE at $T_s = 600$ °C.¹⁹⁾ During the MBE growth, R_{Si} was fixed to be 0.9 nm/min and R_{Ba} was varied from 0.9 to 5.0 nm/min, giving a variation of R_{Ba}/R_{Si} from 1.0 to 5.6. We set the B crucible temperature at 1100 °C for B concentration to be approximately 10^{17} cm⁻³. We then formed a 3-nm-thick a-Si capping layer in situ at 180 °C, which acts as a surface passivation layer.^{26,27)} Finally, indium-tin-oxide (ITO) electrodes with a diameter of 1 mm and a thickness of 80 nm were sputtered on the surface, and Al electrodes were formed on the entire back surface. In this study, we used reflection high-energy electron diffraction (RHEED) and x-ray diffraction (XRD; RIGAKU Smart Lab), Raman spectroscopy (JASCO NRS -5100) equipped with a frequency-doubled Nd:YAG laser (532 nm, 5.1 mW) to characterize crystalline quality of grown films. The time of acquisition for each Raman spectrum was 100 s. The absolute Raman shift was corrected by the transverse optical (TO) phonon line (520.2 cm⁻¹) of crystalline Si.

Photoresponsivity was evaluated using a lock-in technique with a xenon lamp and a 25-cm-focal-length single monochromator (Bunko Keiki SM-1700A and RU-60N). The light intensity was calibrated with a pyroelectric sensor (Melles Griot 13PEM001/J). All measurements were carried out at room temperature (RT).

III. RESULTS AND DISCUSSION

Figure 1 shows the θ - 2θ XRD and RHEED patterns after MBE of B-doped BaSi₂

layers with different values of $R_{\text{Ba}}/R_{\text{Si}}$. Regardless of $R_{\text{Ba}}/R_{\text{Si}}$, a -axis-oriented diffraction peaks of BaSi_2 in the XRD patterns can be observed together with streaky and spot RHEED patterns. This means that a -axis-oriented BaSi_2 films were grown epitaxially on the Si (111) substrates. While sharp streaky RHEED patterns were observed at $R_{\text{Ba}}/R_{\text{Si}} = 1.0 - 3.9$, the sample grown with $R_{\text{Ba}}/R_{\text{Si}} = 5.6$ shows spot RHEED patterns, indicating that the surface of BaSi_2 epitaxial films was not smooth at $R_{\text{Ba}}/R_{\text{Si}} = 5.6$. On the other hand, with the decrease of $R_{\text{Ba}}/R_{\text{Si}}$, thereby for BaSi_2 films grown under Si-rich conditions, the diffraction intensity of each peak gradually decreased, meaning that the crystalline quality of BaSi_2 films was degraded

Figure 2 shows the Raman spectra of BaSi_2 films in the range between 200 and 700 cm^{-1} . We observed five peaks which originate from the internal vibrations of Si tetrahedra in the BaSi_2 lattice.²⁸⁾ For samples grown under Si-rich conditions, $R_{\text{Ba}}/R_{\text{Si}} = 1.0$ and 1.4 , the transverse optical phonon line of Si (Si_{TO}) was observed. The absorption coefficient of BaSi_2 at a wavelength of the excited laser light (532nm) is $\alpha = 3 \times 10^5 \text{ cm}^{-1}$.²⁾ Hence, the penetration depth of the laser light is about $1/\alpha \times 3 \approx 0.1 \mu\text{m}$. This value is much smaller than the BaSi_2 layer thickness. Thus, the Si_{TO} signal was interpreted to originate from Si precipitated in the BaSi_2 films. This is because the BaSi_2 films in these samples were grown under Si-rich conditions. Thus, excess Si atoms might agglomerate to form Si precipitates in the BaSi_2 films.

Figure 3 shows the results of Hall measurements. Depending on $R_{\text{Ba}}/R_{\text{Si}}$, the conduction type and carrier concentration of B-doped BaSi_2 films changed as shown in Fig. 3(a). In the case of B-doped BaSi_2 films with $R_{\text{Ba}}/R_{\text{Si}} = 2.1-2.9$, the conduction type was p-type. At $R_{\text{Ba}}/R_{\text{Si}} = 2.4$, a hole concentration was $2 \times 10^{17} \text{ cm}^{-3}$, and a hole mobility was $112 \text{ cm}^2/\text{Vs}$. The valence band maximum of BaSi_2 is mostly composed of the Si p state in BaSi_2 . Hence, we expect that the replacement of some Si atoms in BaSi_2 by a group 13 element like B will decrease the valence electron concentration and cause BaSi_2 to become p-type semiconductor.^{8-10,29)} On the other hand, for B-doped BaSi_2 films grown under Ba-rich conditions ($R_{\text{Ba}}/R_{\text{Si}} > 3.9$) and Si-rich conditions ($R_{\text{Ba}}/R_{\text{Si}} < 1.4$), the

conduction type was n-type in spite of B doping. We assumed that a large number of V_{Si} gave rise to electrons, and thus the electron concentration became higher than the residual hole concentration caused by B atoms, leading to the formation of n-BaSi₂ films. Note that there is a marked difference in measured mobility between electrons and holes in Fig. 3(b). However, there is not so much difference between them according to theoretical calculations in Ref. [8]; the effective masses of electron and hole are calculated to be $0.41m_0$ and $0.53m_0$, respectively. Here, m_0 is the free electron mass. Therefore, we ascribe such a large difference in mobility to different scattering mechanisms in lightly B-doped BaSi₂ films, discussed in Ref [30].

Figures 4(a) and 4(b) shows photoresponse spectra of undoped BaSi₂ and B-doped BaSi₂ films grown with various values of R_{Ba}/R_{Si} . A bias voltage $V_{bias} = -1.0$ V was applied to the front-surface ITO electrode with respect to the back-surface Al electrode to extract the photogenerated holes in the BaSi₂ films to the ITO electrode. In the case of B-doped BaSi₂ films, the photoresponsivity became a maximum at $R_{Ba}/R_{Si} = 2.1$. As shown in Fig. 2, $R_{Ba}/R_{Si} = 2.1$ is the smallest value below which Si_{ITO} lines marked by red circles appears, meaning the formation of Si precipitates. This trend is the same as those obtained for undoped BaSi₂ films.³¹⁾ In comparison with undoped one, lightly B-doped BaSi₂ films show much higher photoresponsivity as shown in Figs. 4(a) and 4(b). It is reasonable to consider that the carrier lifetime is improved for lightly B-doped BaSi₂ films. In this work, the photoresponsivity of BaSi₂ films was measured using the photoconduction effect. Therefore, the photoresponsivity is roughly proportional to the carrier lifetime.³²⁾ Therefore, we attribute the increase in photoresponsivity to the increase of carrier lifetime by the decrease of point defects in B-doped BaSi₂ films. In undoped BaSi₂ films, photoresponsivity and carrier lifetime improved significantly by hydrogen

(H) passivation.³³⁾ H atoms in BaSi₂ films are considered to inactivate V_{Si}, which are most likely to form in BaSi₂.²³⁾ Likewise, we speculate that doping B atoms make V_{Si} inactive in B-doped BaSi₂ films.

IV. CONCLUSION

We fabricated 0.5- μm -thick lightly B-doped BaSi₂ epitaxial films with different values of $R_{\text{Ba}}/R_{\text{Si}}$, and evaluated their electrical and optical properties. From XRD measurement, the epitaxial growth of *a*-axis-oriented BaSi₂ films were confirmed for all of the samples. The p-BaSi₂ films were formed only at $R_{\text{Ba}}/R_{\text{Si}} = 2.1\text{--}2.9$. From Raman spectroscopy measurement, we found that the Si^{TO} phonon line appeared in B-doped BaSi₂ epitaxial films under the conditions of $R_{\text{Ba}}/R_{\text{Si}} \leq 1.4$. The photoresponsivity was the highest when $R_{\text{Ba}}/R_{\text{Si}}$ was a little larger than the point at which the Si^{TO} peak increased. This result was the same as that obtained for undoped BaSi₂ films. B-doped BaSi₂ epitaxial films at $R_{\text{Ba}}/R_{\text{Si}} = 2.1$ showed higher photoresponsivity than undoped BaSi₂ epitaxial film. Therefore, this result shows that lightly B-doped BaSi₂ films are more promising as a light absorbing layer than undoped BaSi₂ films.

ACKNOWLEDGEMENTS

This work was financially supported by JSPS KAKENHI Grant Numbers 17K18865 and 18H03767. One of the authors (Y.Y.) was financially supported by a Grant-in-Aid for JSPS Fellows (19J21372).

Fig. 1 θ - 2θ XRD and RHEED patterns of B-doped BaSi₂ films with $R_{\text{Ba}}/R_{\text{Si}} = 1.0$ – 5.6 .

Fig. 2 Raman spectra of B-doped BaSi₂ films with $R_{\text{Ba}}/R_{\text{Si}} = 1.0$ – 5.6 . Vibrational modes due to Si tetrahedral in the lattice of BaSi₂ are denoted by Fg, Eg, and Ag. Red broken circles indicate the peak of Si_{TO}.

Fig. 3 (a) Carrier concentration and (b) mobility of B-doped BaSi₂ films as a function of $R_{\text{Ba}}/R_{\text{Si}}$. B-doped BaSi₂ films show p-type conductivity in the $R_{\text{Ba}}/R_{\text{Si}}$ range 2.1 – 2.9 .

Fig. 4 Photoresponse spectra of (a) B-doped BaSi₂ films and (b) undoped BaSi₂ films grown with various values of $R_{\text{Ba}}/R_{\text{Si}}$.

References

- 1) K. Yoshikawa, H. Kawasaki, W. Yoshida, K. Konishi, K. Nakano, T. Uto, D. Adachi, M. Kakematsu, H. Uzu, and K. Yamamoto, *Nat. Energy* **2**, 17032 (2017).
- 2) W. Shockley and H. J. Queisser, *J. Appl. Phys.* **32**, 510 (1961).
- 3) Press Release, Fraunhofer Institute for Solar Energy Systems, 1 December (2014).
- 4) T. Suemasu and N. Usami, *J. Phys. D* **50**, 023001 (2017).
- 5) M. Imai and T. Hirano, *J. Alloys Compd.* **224**, 111 (1995).
- 6) R. A. McKee and F. J. Walker, *Appl. Phys. Lett.* **63**, 2828 (1993).
- 7) K. Toh, T. Saito, and T. Suemasu, *Jpn. J. Appl. Phys.* **50**, 068001 (2011).
- 8) D. B. Migas, V. L. Shaposhnikov, and V. E. Borisenko, *Phys. Status Solidi B* **244**, 2611 (2007).
- 9) M. Kumar, N. Umezawa, and M. Imai, *J. Appl. Phys.* **115**, 203718 (2014).
- 10) M. Kumar, N. Umezawa, and M. Imai, *Appl. Phys. Express* **7**, 071203 (2014).
- 11) M. Baba, K. Toh, K. Toko, N. Saito, N. Yoshizawa, K. Jiptner, T. Sakiguchi, K. O. Hara, N. Usami, and T. Suemasu, *J. Cryst. Growth* **348**, 75 (2012).
- 12) M. A. Khan, K. O. Hara, W. Du, M. Baba, K. Nakamura, M. Suzuno, K. Toko, N. Usami, and T. Suemasu, *Appl. Phys. Lett.* **102**, 112107 (2013).
- 13) M. A. Khan, K. Nakamura, W. Du, K. Toko, N. Usami, and T. Suemasu, *Appl. Phys. Lett.* **104**, 252104 (2014).
- 14) M. Kobayashi, Y. Matsumoto, Y. Ichikawa, D. Tsukada, and T. Suemasu, *Appl. Phys. Express* **1**, 051403 (2008).
- 15) K. O. Hara, N. Usami, K. Toh, M. Baba, K. Toko, and T. Suemasu, *J. Appl. Phys.* **112**, 083108 (2012).
- 16) K. O. Hara, N. Usami, K. Nakamura, R. Takabe, M. Baba, K. Toko, and T. Suemasu, *Appl. Phys.*
- 17) R. Takabe, K. O. Hara, M. Baba, W. Du, N. Shimada, K. Toko, N. Usami, and T. Suemasu, *J. Appl. Phys.* **115**, 193510 (2014).
- 18) S. Yachi, R. Takabe, K. Toko, and T. Suemasu, *Appl. Phys. Lett.* **109**, 072103 (2016).
- 19) D. Tsukahara, S. Yachi, H. Takeuchi, R. Takabe, W. Du, M. Baba, Y. Li, K. Toko, N. Usami, and T. Suemasu, *Appl. Phys. Lett.* **108**, 152101 (2016).
- 20) T. Deng, T. Sato, Z. Xu, R. Takabe, S. Yachi, Y. Yamashita, K. Toko, and T. Suemasu, *Appl. Phys. Express* **11**, 6 (2018).
- 21) K. Kodama, R. Takabe, T. Deng, K. Toko, and T. Suemasu, *Jpn. J. Appl. Phys.* **57**, 050310 (2018).
- 22) K. Kodama, Y. Yamashita, K. Toko, and T. Suemasu, *Appl. Phys. Express* **12**, 041005 (2019).

- 23) M. Kumar, N. Umezawa, W. Zhou, and M. Imai, *J. Mater. Chem. A* **5**, 25293 (2017).
- 24) R. Takabe, T. Deng, K. Kodama, Y. Yamashita, T. Sato, K. Toko, and T. Suemasu, *J. Appl. Phys.* **123**, 045703 (2018).
- 25) Y. Inomata, T. Nakamura, T. Suemasu, and F. Hasegawa, *Jpn. J. Appl. Phys.* **43**, 4155 (2004).
- 26) R. Takabe, S. Yachi, W. Du, D. Tsukahara, H. Takeuchi, K. Toko, and T. Suemasu, *AIP Advances* **6**, 085107 (2016).
- 27) R. Takabe, H. Takeuchi, W. Du, K. Ito, K. Toko, S. Ueda, A. Kimura, and T. Suemasu, *J. Appl. Phys.* **119**, 165304 (2016).
- 28) H. Hoshida, N. Murakoso, T. Suemasu, and Y. Terai, *Defect and Diffusion Forum* **386**, 43 (2018).
- 29) Y. Imai, A. Watanabe, and M. Mukaida, *J. Alloys Compd.* **385**, 257 (2003).
- 30) T. Deng, T. Suemasu, D. A. Shohonov, I. S. Samusevich, A. B. Filonov, D. B. Migas, and V. E. Borisenko, *Thin Solid Films* **661**, 7 (2018).
- 31) Y. Yamashita, T. Sato, K. Toko, A. Uedono, and T. Suemasu, *Appl. Phys. Express* **12**, 055506 (2019).
- 32) S. M. Sze, *Physics of Semiconductor Devices*, 2nd ed. (Wiley, New York, 1981).
- 33) Z. Xu, D. A. Shohonov, A. B. Filonov, K. Gotoh, T. Deng, S. Honda, K. Toko, N. Usami, D. B. Migas, V. E. Borisenko, and T. Suemasu, *Phys. Rev. Mater.* **3**, 065403 (2019).

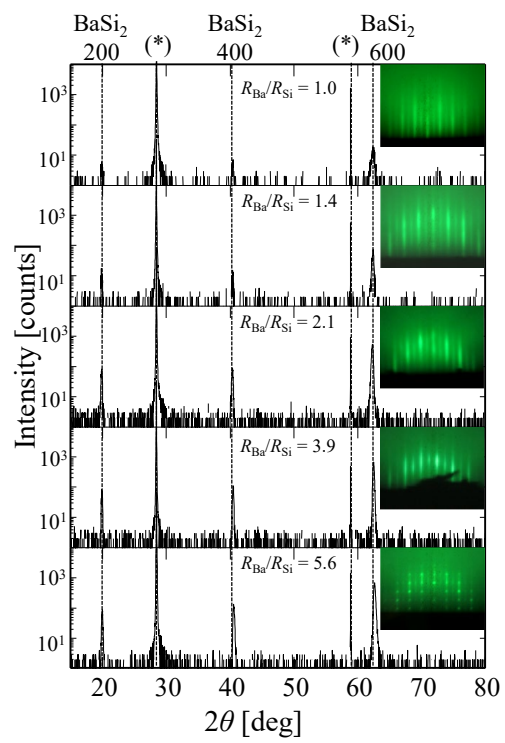


Fig. 1

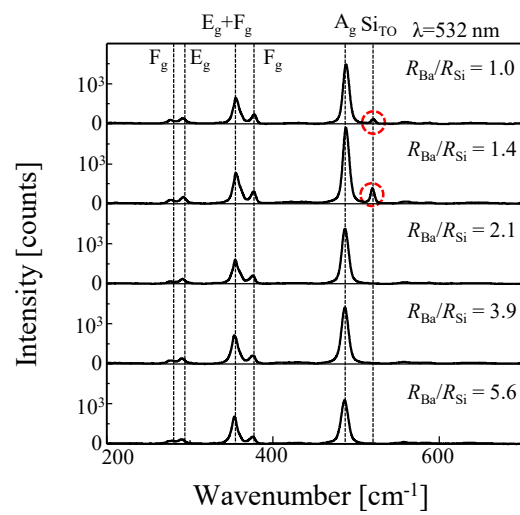


Fig. 2

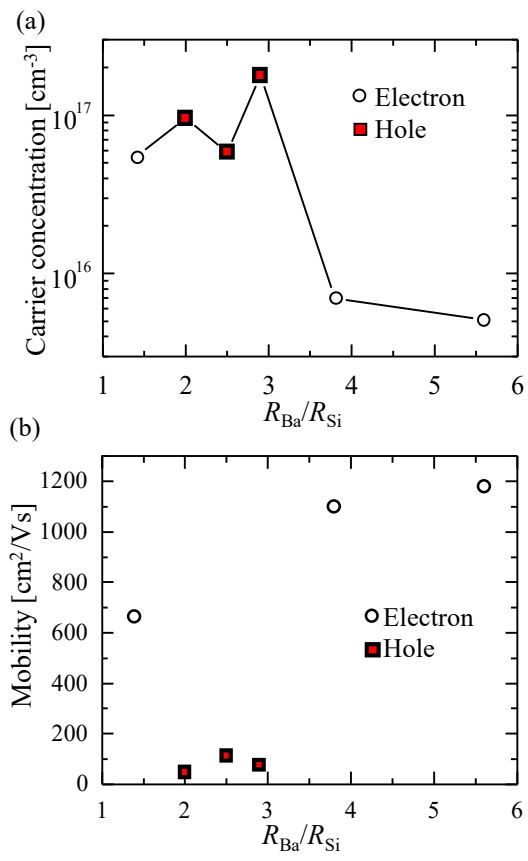


Fig. 3

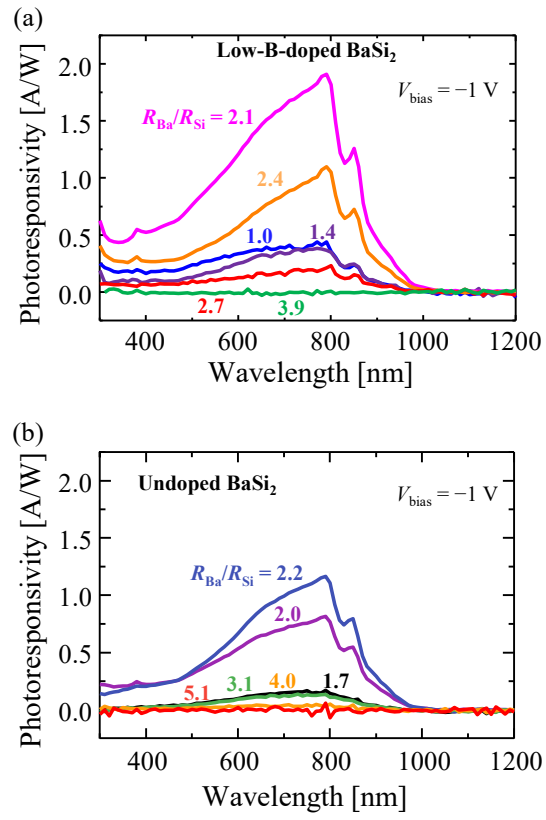


Fig. 4